Phase diagram of a bilinear-biquadratic spin-1 model on the triangular lattice from density matrix renormalization group simulations

Aaron Szasz,* Chong Wang, and Yin-Chen He
Perimeter Institute for Theoretical Physics, Waterloo, Ontario N2L 2Y5, Canada

(Received 20 June 2022; accepted 22 August 2022; published 6 September 2022)

We investigate a highly frustrated spin-1 model on the triangular lattice, with nearest- and next-nearest-neighbor antiferromagnetic $S \cdot S$ interactions and nearest-neighbor $(S \cdot S)^2$ interactions. Using the density matrix renormalization group technique, we find three magnetically ordered phases, namely 120° spiral order, stripe order, and tetrahedral order, as well as two spin nematic phases: ferroquadrupolar and antiferroquadrupolar. While our data could be consistent with a spin liquid phase between the 120° spiral and antiferroquadrupolar orders, the more likely scenario is a direct continuous transition between these two orders.

DOI: 10.1103/PhysRevB.106.115103

I. INTRODUCTION

Geometric frustration of antiferromagnetism can lead to novel phases of matter such as spin liquids, which preserve all symmetries of the system down to zero temperature and feature gapless or topological quasiparticle excitations [1–3]. Such a spin liquid state was first predicted by Anderson in 1973 for the antiferromagnetic nearest-neighbor spin-1/2 Heisenberg model on the triangular lattice [4]. Although that particular model was later shown to realize a three-sublattice magnetic order in the ground state [5,6], in 2003 spin liquid-like behavior was indeed observed in a material approximately described by weakly coupled triangular lattice layers, κ-(BEDT-TTF)$_2$Cu$_2$(CN)$_3$ [7], which was found to have no magnetic ordering down to low temperature. Subsequent experiments demonstrated further properties suggestive of a (possibly topological) spin liquid, including specific heat consistent with gapless low-energy excitations [8] and thermal conductivity consistent with a gapped bulk [9].

As κ-(BEDT-TTF)$_2$Cu$_2$(CN)$_3$ and other spin liquid-candidate materials such as EtMe$_3$Sb[Pd(dmit)$_2$]$_2$ [10–16], YbMgGaO$_4$ [17–19], and herbertsmithite [20,21] have one free electron per effective lattice site, theory work has largely focused on the half-filled Hubbard model and its strong-coupling limit, the spin-1/2 Heisenberg model with higher-order terms beyond nearest neighbor. Recent numerical studies confirm that these models indeed have spin liquid ground states, including chiral spin liquids and Dirac spin liquids on the triangular [22–28] and kagome lattices [29–33].

There are also materials realizing higher-spin frustrated antiferromagnets. In 2005, Nakatsuji *et al.* discovered a possible spin-liquid candidate material that can be approximately described by a spin-1 triangular lattice, NiGa$_2$S$_4$, which also shows a lack of magnetic order down to low temperature [34–40]. First-principles electronic structure calculations and other methods have suggested that NiGa$_2$S$_4$ has strong third-neighbor Heisenberg (bilinear) interactions, as well as significant nearest-neighbor and possibly second-neighbor interactions [41–45]. Furthermore, the most general two-body interactions for spin-1 systems include $(\mathbf{S} \cdot \mathbf{S})^2$ (biquadratic) interactions [46], which are believed to be significant in a variety of materials [47]; following an initial proposal by Tsunetsugu and Arikawa [48], nearest-neighbor biquadratic interactions are typically included in phenomenological models of NiGa$_2$S$_4$.

The spin-1 triangular lattice model with nearest-neighbor bilinear and biquadratic terms has been studied extensively since the mid-2000s and has been shown to host four phases: the same three-sublattice magnetic order found in the spin-1/2 triangular lattice, ferromagnetic order, and two types of nematic order [49–52]. These nematic states have been proposed to explain the behavior of NiGa$_2$S$_4$ [48,53,54], but the matter remains unresolved.

One of our goals in the present work is to generalize these spin-1 triangular lattice studies by incorporating longer-ranged interactions. The specific model we study is presented in Eq. (1) below; in summary, the model has antiferromagnetic Heisenberg (bilinear) interactions between nearest and next-nearest neighbors and biquadratic interactions (of both signs) between nearest neighbors. While we consider a second-neighbor interaction rather than the (in principle more relevant to NiGa$_2$S$_4$) third-neighbor interaction, our results still shed light on how the nearest-neighbor-only phase diagram changes when additional terms are included. Additionally, second-neighbor interactions may be relevant to other spin-1 triangular lattice systems, including the spin liquid candidate Ba$_3$NiSb$_2$O$_9$ [55–60] and materials with magnetic ground states such as Ba$_2$La$_2$NiTe$_2$O$_{12}$ [61], Na$_2$BaNi(PO$_4$)$_2$ [62], and FeI$_2$ [63].

We have two key motivations for including specifically the second-neighbor interaction. First, a large-S expansion of precisely this model shows the possible appearance of a quantum disordered phase as S becomes small [64]. Second, we aimed to study a model that could feature a Stiefel liquid; Stiefel liquids are a recently predicted novel class of

*aszasz@perimeterinstitute.ca

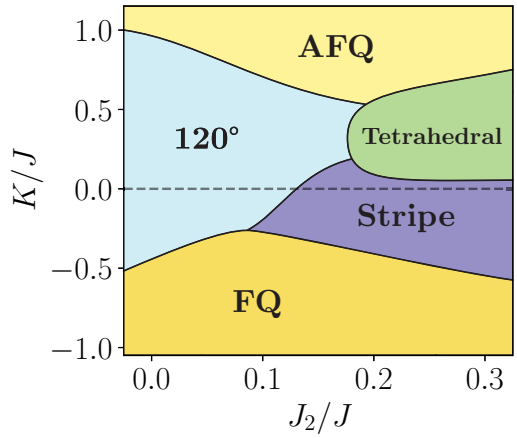

FIG. 1. Phase diagram of spin 1s on the triangular lattice with three competing interactions, based on simulations on a circumference-six cylinder with YC boundary conditions. Axes are strength of next-nearest-neighbor interactions, J_2, and nearest-neighbor biquadratic interactions, K, relative to antiferromagnetic nearest-neighbor interactions, J. There are three magnetic orders (120°, stripe, and tetrahedral) and two nematic orders, ferro-quadrupolar (FQ) and antiferroquadrupolar (AFQ). We do not find a disordered phase.

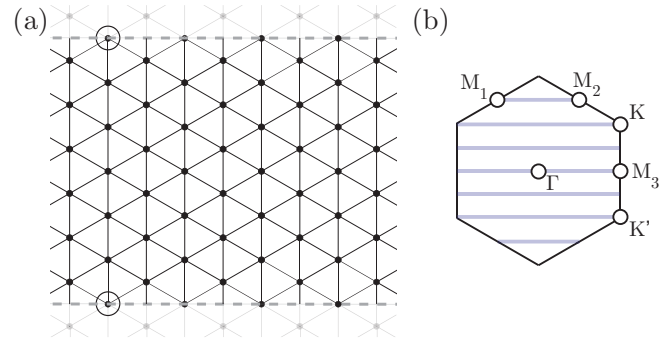

FIG. 2. (a) The YC6 triangular lattice. There are periodic boundary conditions in the direction along the vertical bond, so that the two dashed lines are identified together to form a cylinder. The two circled points are equivalent. (b) The corresponding Brillouin zone. The finite circumference cylinder restricts k_y to lie on the horizontal cuts shown. For the YC6 cylinder in particular, these cuts contain all the high-symmetry points indicated in the figure: Γ at the zone center, K and K′ at the corners, and the three M points at the centers of the edges.

disordered quantum phases generalizing the Dirac spin liquid and deconfined quantum critical point [65,66]. The simplest never-yet-observed example of a Stiefel liquid should occur in proximity to the non-co-planar tetrahedral magnetic order [65], while another Stiefel liquid could arise near a nematic phase [66]. The spin-1 model we consider is expected, based on the large-S predictions and past results on the nearest-neighbor model, to host both ordered phases, and hence could plausibly realize these Stiefel liquids.

We study the extended bilinear-biquadratic model using density matrix renormalization group (DMRG) [67–70] simulations on infinitely-long finite circumference cylinders; DMRG finds the lowest energy state within the variational class of matrix product states (MPS). We find precisely all five expected phases, namely the three magnetic orders (120°, stripe, tetrahedral) from the classical limit and the two nematic orders (ferroquadrupolar, antiferroquadrupolar) found in the limit of no second-neighbor interaction. Our phase diagram is shown in Fig. 1. Our results are plausibly consistent with a disordered phase, which could be a spin liquid, between the 120° and antiferroquadrupolar phases, but there is no compelling evidence favoring this interpretation over a direct continuous phase transition. Our results do suggest that there is no first-order transition between these phases, in contrast to the conclusions of some previous works [51,52].

The remainder of the paper is organized as follows. In Sec. II, we introduce our model and comment on our DMRG implementation. We also provide a review of both spin-quadrupole order and past results from the literature. In Sec. III we present detailed results from our simulations, including key data such as structure factors and correlation lengths that we use to identify the phases and locate their boundaries; we explain why we interpret our data as indicating the absence of a disordered phase. Finally, in Sec. IV, we summarize our findings and discuss possible modifications to the model that could lead to spin liquid ground states.

II. THE MODEL

We study spin-1 degrees of freedom on the triangular lattice, with the Hamiltonian

$$H = \sum_{\langle ij\rangle} [J\,\mathbf{S}_i \cdot \mathbf{S}_j + K(\mathbf{S}_i \cdot \mathbf{S}_j)^2] + J_2 \sum_{\langle\langle ij\rangle\rangle} \mathbf{S}_i \cdot \mathbf{S}_j, \quad (1)$$

where $\langle ij\rangle$ denotes pairs of nearest-neighbor sites and $\langle\langle ij\rangle\rangle$ denotes next-nearest neighbors; $\mathbf{S}$ on each site is the usual spin-1 operator. We consider only the case of $J, J_2 > 0$, but allow K to have both signs. Throughout the paper, we refer to the $\mathbf{S}\cdot\mathbf{S}$ and $(\mathbf{S}\cdot\mathbf{S})^2$ interactions as bilinear and biquadratic, respectively.

We study this model using DMRG simulations on infinite cylinders with a finite circumference of six sites, using YC boundary conditions [24] as shown in Fig. 2(a). We improve the efficiency of our simulation by using delinearization [71] to perform lossless compression of the matrix product operator representation of H. In momentum space, the finite cylinder circumference discretizes the allowed momentum in the direction around the cylinder. In Fig. 2(b), we show the allowed momenta in the Brillouin zone for the cylinder we consider. Importantly, the allowed momentum cuts for the YC6 cylinder include all high-symmetry points in the Brillouin zone, namely the M, K, and Γ points as labeled in the figure.

Before proceeding to discuss our findings, we review the expected behavior of the model, in limiting cases and based on results from the literature.

A. Limiting cases and quadrupolar order

We consider the following three limits of the model: $J > 0$ only, $K > 0$ only, and $K < 0$ only. We also discuss the parameter point $J = K$, $J_2 = 0$, where there is an emergent larger global symmetry group.

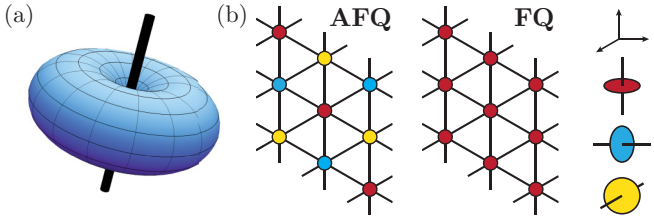

FIG. 3. (a) A visualization of single-site spin-quadrupole order. The distance of the surface from the origin in each direction $\hat{n}$ shows $\langle(\hat{n}\cdot\mathbf{S})^2\rangle$. Spin fluctuations are small along the "director" and large in the two perpendicular directions. (b) AFQ and FQ order on the triangular lattice. The cartoon picture of AFQ order is a three-sublattice product state of single-site quadrupoles; the director is the same for all sites within a sublattice, and the directors on the three sublattices lie along three orthogonal directions. The quadrupole structure factor has peaks at the K points. The cartoon picture of the FQ order is a product state of single-site quadrupoles with parallel directors on all sites. The quadrupole structure factor has a peak at the Γ point.

For the pure nearest-neighbor Heisenberg antiferromagnet, with $K = J_2 = 0$, the ground state has 120° three-sublattice magnetic order. This is the classical (large-S) ground state and has also been established by various numerical methods, including exact diagonalization [49], cluster mean-field theory [50], and tensor network simulations [51,52], as the ground state for spin 1. In momentum space, the spin structure factor

$$S(\mathbf{q}) = \frac{1}{N}\sum_{ij} e^{i\mathbf{q}\cdot\mathbf{r}_{ij}}\langle\mathbf{S}_i\mathbf{S}_j\rangle \tag{2}$$

has peaks at the K and K′ points at the corners of the hexagonal Brillouin zone.

More interesting is the purely biquadratic Hamiltonian, with $J = J_2 = 0$, which gives rise to spin-nematic order [72–76]. Like a magnetically ordered state, a spin-nematic state breaks spin rotation symmetry; unlike a magnetic state, it preserves time reversal. This combination is possible if the spin dipole moment is zero, but higher-order multipoles are nonzero. Quadrupole order in particular is very natural for spin 1, as we now explain.

The key insight is that each spin-1 Hilbert space has an orthonormal basis of spin-quadrupole states, namely the 0-eigenvectors of $\hat{n}\cdot\mathbf{S}$ along any three orthogonal directions. For example, the 0-eigenvectors of S_z, S_x, and S_y are, when written in the z basis, $|z\rangle \equiv -i(0,1,0)^T$, $|x\rangle \equiv (i,0,-i)^T/\sqrt{2}$, and $|y\rangle \equiv (1,0,1)^T/\sqrt{2}$; the somewhat strange coefficients are chosen for convenience, following Ref. [49].

Each of these 0-eigenvectors is a single-site (quadrupolar) nematic state. Consider, for example, $|z\rangle$. This state has $\langle z|\hat{n}\cdot\mathbf{S}|z\rangle = 0$ for all $\hat{n}$, so time-reversal symmetry is not broken; however, $\langle z|(\hat{n}\cdot\mathbf{S})^2|z\rangle = \sin^2(\theta)$ where θ is the angle between $\hat{z}$ and $\hat{n}$. As illustrated in Fig. 3(a), spin-rotation symmetry is broken to the symmetry of an ellipsoid, which has a quadrupole moment but no dipole moment. More generally, the state $|n\rangle = \hat{n}\cdot(|x\rangle,|y\rangle,|z\rangle)$, for any real unit vector $\hat{n}$, is the 0-eigenstate of $\hat{n}\cdot\mathbf{S}$, and hence is likewise a spin-quadrupole. The direction with no spin fluctuations, $\pm\hat{n}$, is called the "director" of the nematic state.

To more precisely characterize quadrupolar nematic order, we use the spin-quadrupole operator $\mathbf{Q}$ given by

$$\frac{Q_{\alpha\beta}}{\sqrt{2}} = \frac{S_\alpha S_\beta + S_\beta S_\alpha}{2} - \frac{S(S+1)}{3}\delta_{\alpha\beta}\mathrm{Id}, \tag{3}$$

for $\alpha,\beta \in \{x,y,z\}$, a traceless symmetric rank-2 tensor [77]. The symmetry and trace conditions imply there are only five independent components, so $\mathbf{Q}$ can equivalently be written as the vector:

$$\mathbf{Q}_v = \begin{pmatrix} S_x^2 - S_y^2 \\ \left(2S_z^2 - S_x^2 - S_y^2\right)/\sqrt{3} \\ \{S_x, S_y\} \\ \{S_y, S_z\} \\ \{S_x, S_z\} \end{pmatrix} \tag{4}$$

with $\{\,,\}$ the anticommutator. The square of the quadrupole operator is $\mathrm{Tr}[\mathbf{QQ}] = \mathbf{Q}_v\cdot\mathbf{Q}_v = (10/3)\mathrm{Id}$. (Note that the trace is taken over the components of the operator-valued matrix $\mathbf{Q}^2$, and not over the spin operators.) The maximum single-site quadrupole moment is $|\langle\mathbf{Q}_v\rangle| \leqslant \sqrt{4/3}$ [78]; the maximum is achieved by the basis state $|z\rangle$, which has $\langle\mathbf{Q}_v\rangle = (0,-\sqrt{4/3},0,0,0)$.

Let us now consider the interaction $(\mathbf{S}\cdot\mathbf{S})^2$. We can write this as [79]

$$(\mathbf{S}\cdot\mathbf{S})^2 = 1 + 3|S\rangle\langle S|, \quad |S\rangle = \frac{|zz\rangle + |xx\rangle + |yy\rangle}{\sqrt{3}}. \tag{5}$$

The projector $P = |S\rangle\langle S|$ is positive semidefinite, so when $K > 0$ the ground state will be in the space projected out by P on every pair of sites. Thus any product state where each site is in the state $|x\rangle$, $|y\rangle$, or $|z\rangle$, and where no two nearest neighbors are in the same state, will be a ground state. We produce such a state on the triangular lattice by identifying three sublattices and placing $|x\rangle$ on each site of one sublattice, and likewise for $|y\rangle$ and $|z\rangle$ on the other two sublattices, as shown in Fig. 3(b). The ordering of this state is referred to as antiferroquadrupolar (AFQ). In momentum space, it is characterized by the quadrupolar structure factor,

$$Q(\mathbf{q}) = \frac{1}{N}\sum_{ij} e^{i\mathbf{q}\cdot\mathbf{r}_{ij}}\langle\mathrm{Tr}[\mathbf{Q}_i\mathbf{Q}_j]\rangle, \tag{6}$$

which has peaks at the K points.

However, the ground state space also contains ferromagnetic (FM) states. For example, the state $|1\rangle_z \equiv (|y\rangle - i|x\rangle)/\sqrt{2}$, with $S_z = 1$, has $P(|1\rangle_z \otimes |1\rangle_z) = 0$, so the fully magnetized state with $|1\rangle_z$ on every site is also a ground state. Thus the pure $K > 0$ model has an exact degeneracy between FM and AFQ order. Infinitesimal nearest-neighbor bilinear interactions break the degeneracy: $J > 0$ gives AFQ order, while $J < 0$ gives FM order, and the transition is first order. We consider only $J > 0$, so we expect AFQ order in the large-K limit.

When $K < 0$, a classical or large-S ground state would be any in which each spin points either parallel or antiparallel to its neighbors, behavior which we call ferronematic or ferroquadrupolar (FQ). In the case of spin-1, a product state will no longer be a ground state, but sign-free quantum Monte Carlo (QMC) calculations provide clear evidence that the ground state remains FQ [79]. The prototypical FQ state for spin-1 is

the product state with $|z\rangle$ on every site, which has a quadrupole structure factor with a peak at the Γ point, $\mathbf{k} = \mathbf{0}$; this state is shown in Fig. 3(b). From the QMC results, the FQ ground state in the pure $K < 0$ model is in the same phase as this product state, but with magnitude of the quadupolar structure factor reduced by about 50%.

There is one more important parameter point to consider, namely $J_2 = 0, J = K$. To demonstrate the significance of this parameter point, we rewrite the biquadratic interaction as

$$(\mathbf{S}_i \cdot \mathbf{S}_j)^2 = \frac{\mathbf{Q}_{vi} \cdot \mathbf{Q}_{vj}}{2} - \frac{\mathbf{S}_i \cdot \mathbf{S}_j}{2} + \frac{4}{3}, \tag{7}$$

in which case the Hamiltonian becomes, for $J_2 = 0$,

$$H = \sum_{\langle ij \rangle} \left(J - \frac{K}{2}\right)\mathbf{S}_i \cdot \mathbf{S}_j + \frac{K}{2}\mathbf{Q}_{vi} \cdot \mathbf{Q}_{vj} + \frac{4}{3}. \tag{8}$$

Following Ref. [49], when $J = K$ we can further combine the spin and quadrupole operators to get

$$\mathbf{S}_i \cdot \mathbf{S}_j + \mathbf{Q}_{vi} \cdot \mathbf{Q}_{vj} = 2W_{ij} - (2/3)\mathrm{Id}, \tag{9}$$

where W_{ij} is the operator that swaps the states of spins i and j, $W_{ij} = \sum_{\alpha\beta} |\alpha\rangle_i |\beta\rangle_j \langle\beta|_i \langle\alpha|_j$ where α and β index basis states for the two spins. The swap operator is invariant under conjugation by $U \otimes U$ for any $U \in \mathrm{SU}(3)$:

$(U^\dagger \otimes U^\dagger) W (U \otimes U) =$ 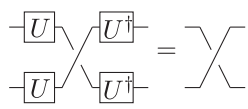 $= W.$ (10)

Thus when $J_2 = 0$ and $J = K$, the Hamiltonian has an emergent SU(3) symmetry group [80].

For another perspective on the SU(3)-symmetric point, we follow Ref. [51], noting that, when written in the basis $\{|x\rangle, |y\rangle, |z\rangle\}$, the three components of $\mathbf{S}$ and five components of $\mathbf{Q}_v$ are given by the eight Gell-Mann matrices [81], generators of SU(3). Thus at the point $J_2 = 0$, $J = K$, the Hamiltonian is given by $(J/2)\sum_{\langle ij \rangle} \boldsymbol{\lambda}_i \cdot \boldsymbol{\lambda}_j$, up to a constant. This Hamiltonian is an SU(3) analog of the spin-1/2 Heisenberg model: we simply replace the vector $\boldsymbol{\sigma}$ of SU(2) generators by vector $\boldsymbol{\lambda}$ of SU(3) generators.

From this formulation of H, it follows that at the SU(3) point, spin-dipole and spin-quadrupole operators must have equal correlation length. As a result, nematic order cannot extend to $K < J$, while magnetic order cannot extend to $K > J$. Two possibilities remain: either there is a direct transition between the two orders at precisely the SU(3)-symmetric point or there is an intermediate phase.

B. Past work

The spin-1 Hamiltonian on the triangular lattice with nearest-neighbor bilinear and biquadratic interactions, but no longer-ranged interactions, has been studied extensively, and there is a broad consensus on the ground state phase diagram. Including both positive and negative J and K, there are four phases: FM, 120° antiferromagnet (AFM), FQ, and AFQ; of these, the FM order exists only for $J < 0$, a case we do not consider in the present study. We now briefly summarize the papers in which these results are presented.

Following the discovery of a nonmagnetic ground state in $NiGa_2S_4$ [34], Tsunetsugu and Arikawa considered the biquadratic interactions and showed using mean-field theory (MFT) that the $K > J > 0$ model has an AFQ ground state [48,54]. Likewise, Bhattacharjee *et al.* showed that $K < 0$, $|K| \gtrsim 1.14J > 0$ gives rise to a FQ ground state in MFT [53]; they found a first-order transition to 120° magnetic order at $K \approx -1.14J$. These works also considered the low-energy excitation spectrum, finding T^2 specific heat in both quadrupolar phases, in agreement with the experiments on $NiGa_2S_4$. The low-lying excitations were also addressed using similar mean-field methods by Li *et al.* [82] and using a continuum field-theory approach by Smerald and Shannon [83].

A number of works have considered the full $J - K$ phase diagram, using a variety of methods. Läuchli *et al.* showed that both MFT and exact diagonalization (ED) on clusters up to 21 sites give the four phases listed above; however, in the ED calculation the FQ order is stabilized relative to AFM order, so the transition occurs at $K \approx -0.4J$ [49]. They also used flavor-wave theory [76] to study excitations, and they considered the effects of applied external magnetic fields. Similar results to the ED were obtained by Moreno-Cardoner *et al.* using cluster MFT with clusters of at least nine sites [50]. More recently, Niesen and Corboz studied the model using infinite projected entangled pair state (iPEPS) simulations [51,52]. They again observe the same four phases, finding the FQ to AFM phase transition at $K \approx -0.42J$.

Some numerical studies have also targeted particularly important parameter points. At the $J = 0, K < 0$ point, with pure biquadratic interactions, Kaul showed using sign-free QMC simulations that the ground state has FQ order [79]. At the SU(3)-symmetric point, $J = K$, Bauer *et al.* found long-ranged quadrupolar order using a combination of flavor-wave theory, DMRG on finite clusters, and iPEPS simulations with four- and nine-site unit cells [84]. Zhang *et al.* likewise found indications of long-ranged nematic order at the SU(3) point using DMRG on finite-length cylinders of circumference 6 and 9 [85]. (In contrast, these two studies disagree on the ground state of the SU(3)-symmetric model on the square lattice: Ref. [84] finds long-ranged order, whereas Ref. [85] and other recent works by the same authors [86,87] do not.)

A number of studies have added single-ion anisotropy to the model, a term of the form $D\sum(S_i^z)^2$, employing methods including MFT [53], fermionic parton MFT [88,89], cluster MFT [50], Schwinger bosons and DMRG [90], and flavor-wave theory [63,91]. These works, as well as a quaternion gauge theory calculation on the pure $J - K$ model [92], suggest a spin liquid ground state is possible, though it may require the addition of ring exchange [88] or anisotropy in the spin interactions [90,91].

Finally, some works have studied the effects of longer-ranged interactions. The $J - K - J_3$ model has been studied using a semiclassical approximation [93], and with fermionic parton MFT [94], suggesting spin-glass-like behavior and a possible spin liquid ground state, respectively. The pure $J - J_2$ model has been studied using a Green's function approach, giving the following phases, in order of increasing J_2: 120° AFM, disordered, stripe magnetic order, incommensurate magnetic order, and three intercollated 120° orders [95]; the first three of these are predicted in the range of J_2 we consider in the present work. The only work we are aware of

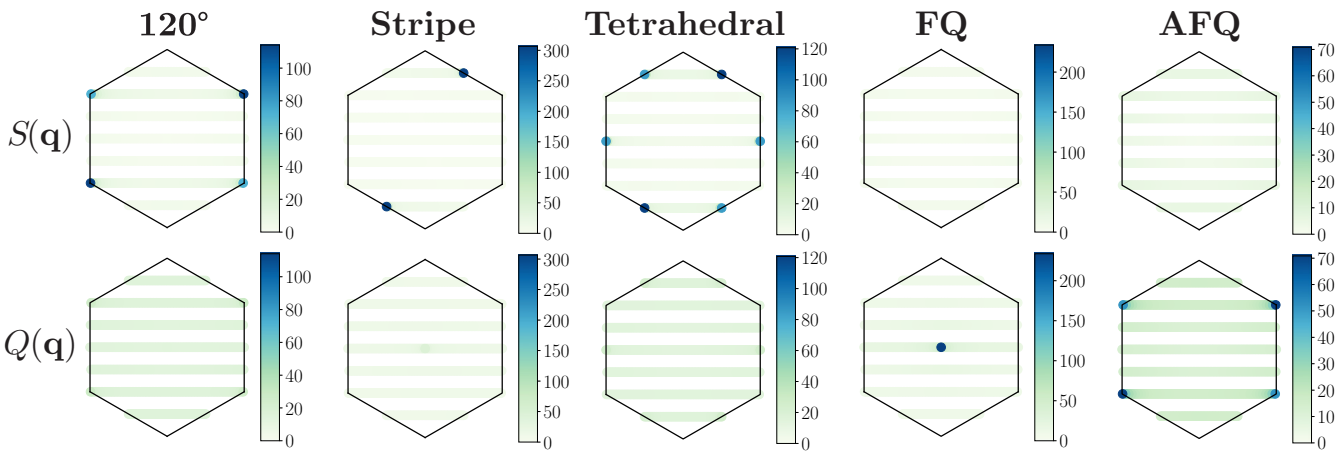

FIG. 4. Top row: Spin structure factor $S(\mathbf{q})$ on allowed momentum cuts at one representative point in each phase: respectively, $(J_2/J, K/J) = (0, 0.2)$, $(0.3, -0.1)$, $(0.3, 0.2)$, $(0.1, -1.0)$, and (0.1,1.0). Structure factors are computed using correlations up to 50 unit cells along the cylinder. Bottom row: Corresponding quadrupole structure factors, $Q(\mathbf{q})$. Note that the scale indicated in the colorbar is consistent between the two structure factors for each phase, clearly indicating whether dipolar or quadrupolar order is dominant, but is different between phases. All structure factors are computed at bond dimension $\chi = 2000$, for which the lowest-energy MPS can spontaneously break spin-rotation symmetry, as discussed in the Appendix; this symmetry-breaking leads to the very large peaks in the structure factors.

that studies the full $J - K - J_2$ triangular-lattice model does so using a large-S expansion [64], and does not consider $S = 1$ in particular. The predicted large-S phases are the 120° AFM when J dominates, stripe order for sufficiently large $K < 0$ and $J_2 > J/8 - 9|K|/16$, and tetrahedral order for $K > 0$ and $J_2 > J/8 - 5K/48$. The authors suggest possible quantum-disordered phases for small S for both signs of K, near the boundaries of the AFM phase.

III. PHASE DIAGRAM AND DATA

The phase diagram we find is summarized in Fig. 1. In short, we find the expected ordered phases: 120° AFM, stripe, and tetrahedral magnetic orders from the classical limit, as well as the expected nematic FQ and AFQ phases. Our data are plausibly consistent with a disordered phase, but more likely no such phase is present. Our data suggest the transition between AFM and AFQ orders may be continuous, which is contrary to the conclusions of some past works discussed above.

Here we present key numerical data on which our summary phase diagram is based and explain how we identify each phase. Figure 4 shows the spin and quadrupolar structure factors, as defined in Eqs. (2) and (6) above, at one representative parameter point in each phase. The structure factors are computed using correlation functions up to a distance of 50 rings along the cylinder. Figure 5 provides a different perspective on the structure factors; we plot the values of $S(\mathbf{q})$ and $Q(\mathbf{q})$ at high-symmetry points in the Brillouin zone across the full parameter space, allowing us to map out the locations of the phases and the transitions between them. Figure 5 also shows the scalar chiral order parameter $\langle \mathbf{S} \cdot (\mathbf{S} \times \mathbf{S}) \rangle$.

The data in both figures are from simulations with a single MPS bond dimension, $\chi = 2000$. The main effect of finite bond dimension is that spin-rotation symmetry is spontaneously broken throughout much of the parameter space we study; this symmetry-breaking seems to violate the Mermin-Wagner theorem, which says that a continuous symmetry cannot be spontaneously broken in the ground state of a one-dimensional quantum system such as a finite-circumference cylinder. However, as we explain in the Appendix, breaking symmetry lowers entanglement and thus can also reduce the energy of variational tensor network states; if this energy benefit exceeds the gap between symmetric and symmetry-broken states, then the symmetry will indeed be spontaneously broken.

Apart from the spontaneous symmetry breaking (SSB), the phase diagram at $\chi = 2000$ is qualitatively correct. Compared with $\chi = 1000$, for which we show the equivalent of Figs. 4 and 5 in the Supplementary Material [96], the only changes are small shifts in phase boundaries and a slightly larger region where spin-rotation symmetry is preserved. Higher-χ data along $J_2/J = 0$ and $J_2/J = 0.1$ cuts through parameter space show that there is likewise no qualitative change as we further increase χ to 4000. Specifically, we observe consistent behavior in both the structure factors (Figs. 6 and 7) and correlation lengths (Fig. 8).

We provide further data in the Supplementary Material [96], including real-space spin correlations, spin-resolved correlation lengths, transfer matrix spectra, and entanglement spectra [97] in each phase; while these are not necessary in order to identify the phases, they provide useful additional confirmation of our conclusions.

In the remainder of this section, we proceed phase by phase, using the data in the figures to identify each one. We also separately discuss the nature of the AFM-AFQ transition; some data in the region around the transition are suggestive of a disordered spin liquid phase, and we explain why we believe this interpretation is not correct.

A. Identification of each phase

1. 120° *AFM*

The spin structure factor in Fig. 4 has clear peaks at the corners of the Brillouin zone, consistent with three-sublattice magnetic order. The extent of the phase is clearly identifiable

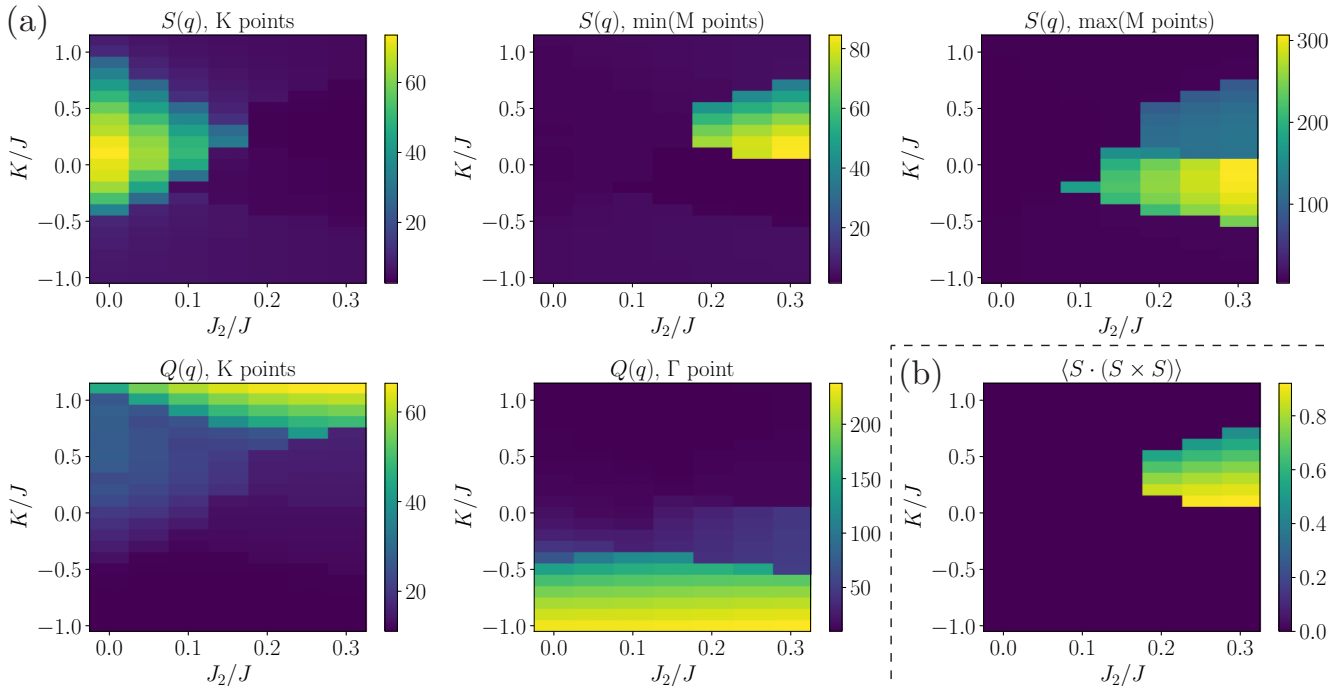

FIG. 5. Data from DMRG simulations with bond dimension $\chi = 2000$. (a) Height of spin and quadrupole structure factors at specific high-symmetry points in the Brillouin zone (see Fig. 2), as a function of J_2/J and K/J. The five ordered phases can be visually identified by these data, as explained in the main text. (b) Scalar chiral order parameter, which is nonzero for tetrahedral magnetic order.

in Fig. 5(a) from $S(q)$ at the K points. We note that the phase includes part of the region $0.04 \lesssim J_2/J \lesssim 0.25$, where the ground state for $K = 0$ was predicted in Ref. [95] to be disordered; while we cannot entirely rule out a disordered ground state in the full two-dimensional model, we find no indication of such behavior.

2. Stripe order

Stripe magnetic order has spins parallel along one lattice vector, and antiparallel along the other; see the Supplementary Material [96] for a real-space picture. In momentum space, the stripe order has a peak at one of the three M points, as shown in Fig. 4. In Fig. 5(a), we identify the phase as the region where the minimum over the three M points is small but the maximum is large. (Note that when we run our simulations independently at each parameter point, the M point at which ordering occurs is chosen spontaneously and is different at different parameter points, but the magnitude of the order parameter is consistent regardless of the choice.)

3. Tetrahedral order

The tetrahedral order is a four-sublattice non-co-planar order, featuring spin ordering at all three M points and a nonzero scalar chirality, as measured by the order parameter $\langle \mathbf{S} \cdot (\mathbf{S} \times \mathbf{S}) \rangle$. We thus identify the extent of this phase from the region with nonzero scalar chirality in Fig. 5(b), which also corresponds to the region with significant ordering at all three M points as indicated by the minimum of the structure factor height over the three points, Fig. 5(a).

4. FQ

The ferroquadrupolar phase has no spin ordering, so the spin structure factor should be small. However, there is quadrupolar nematic order with the director parallel on all sites, so that the quadrupolar order parameter should have a peak at $\mathbf{k} = \mathbf{0}$. Precisely this behavior is shown in the structure factors at $(J_2/J, K/J) = (0.1, -1)$ in Fig. 4, and we can see the extent of the phase from $Q(q)$ at the Γ point in Fig. 5(a). As we explain in the Supplementary Material [96], at each parameter point in this phase we actually find two nearly degenerate ground states. These correspond to two different ways of spontaneously breaking symmetry due to competition between energy and entanglement (see Appendix), and the true infinite bond dimension ground state is symmetric and unique.

5. AFQ

This phase will again have a small spin structure factor but a large quadrupolar structure factor, now with peaks at the K points. We show the structure factors at $(J_2/J, K/J) = (0.1, 1.0)$ in Fig. 4, exhibiting precisely this expected behavior. The extent of the phase can be seen from $Q(q)$ at the K points in Fig. 5(a). However, these data do not indicate the full phase; rather, the visually distinct region in the figure corresponds only to the portion of the phase where the symmetry is spontaneously broken. The full phase extends to smaller K, and we identify the full extent of the phase as the region where the quadrupolar structure factor is largest at the K points and the spin-2 correlation length is larger than the spin-1 correlation length (see Fig. 8).

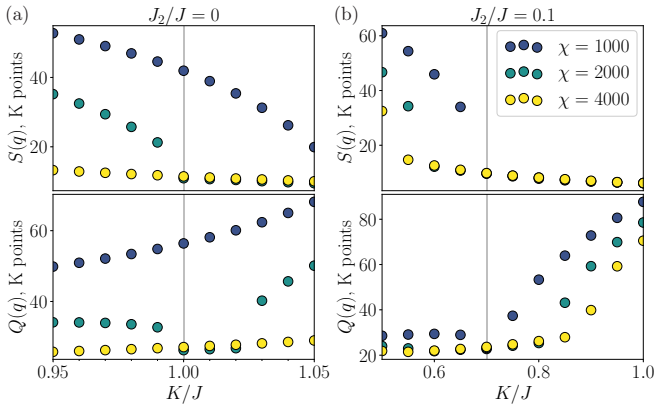

FIG. 6. Height of spin- and quadrupole-structure factors at the K points, as a function of K/J with (a) $J_2 = 0$ and (b) $J_2/J = 0.1$. Simulations were carried out with a three-ring unit cell, allowing for explicit symmetry-breaking realizing the three-sublattice AFM and AFQ orders. We observe such symmetry breaking at smaller bond dimension, and the symmetry is restored as χ increases.

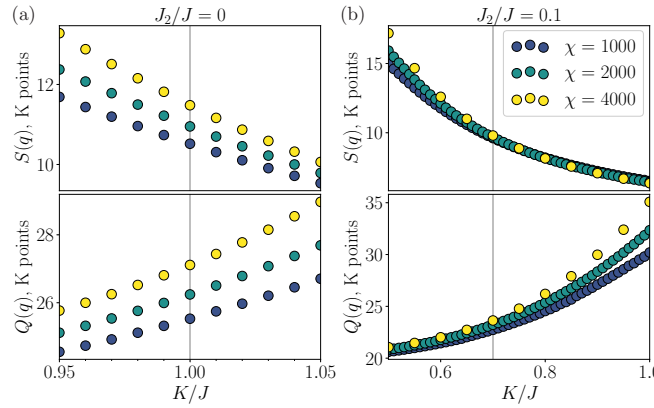

FIG. 7. Height of spin- and quadrupole-structure factors at the K points, as a function of K/J with (a) $J_2 = 0$ and (b) $J_2/J = 0.1$. Simulations were carried out with a one-ring unit cell, so that explicit symmetry-breaking realizing a three-sublattice order is disallowed. The lowest-energy MPS exactly matches the result for the three-ring unit cell once the bond dimension is large enough in the latter case to restore the symmetry. In this case the presence of long-range order is not at all clear; however, especially at $J_2/J = 0.1$, it appears that each of spin and quadrupole order is converged with bond dimension on one side of $K/J \approx 0.7$ and not on the other.

B. AFM-AFQ phase transition vs spin liquid

Finally, we focus on the phase transition between the two three-sublattice orders, AFQ and 120° AFM. In two dimensions, spin-rotation is spontaneously broken in the true ground state, so one can simply find where the local spin moment goes to 0 to identify the boundary of the AFM phase as in Ref. [52]; the quadrupolar order will be nonzero even in the AFM phase [93], but a sharp decrease would still make the phase boundary clear.

In contrast, on the cylinder the true $\chi = \infty$ ground state preserves all symmetries on both sides of the transition. If the transition is first order, then there could be significant ordering even infinitesimally away from the transition and thus a very small energy cost to break the symmetry, so that the energy benefit of reduced entanglement can lead to SSB at even sizable bond dimensions (see Appendix). However, if the transition is continuous or weakly first order, then breaking symmetry in favor of the order on one side (say, AFQ) will impose a significant energy cost due to the resulting lack of short-range correlations corresponding to the other order (correspondingly, AFM). Thus we would expect symmetry to be preserved starting from relatively modest bond dimensions.

As a result, the same numerical data, namely a small region of symmetry-preserving ground states with no long-range order, even at modest bond dimension, is consistent with two possibilities: a disordered region or a direct continuous (or weakly first-order) transition. On a single finite-circumference cylinder, there is no rigorous way to distinguish these two possibilities. This is precisely the phenomenology we observe, as shown for the spin-structure factor with a three-ring unit cell in Fig. 6. At each sufficiently large bond dimension, there is a region at both $J_2/J = 0$ and $J_2/J = 0.1$ for which symmetry is preserved and there is no long-range order. In this region, the ground state exactly matches the results of simulations with a one-ring unit cell, shown in Fig. 7, for which three-sublattice symmetry-breaking is disallowed.

However, there are several reasons to believe that there is not in fact a disordered phase between the AFM and AFQ orders:

(1) Considering the $J_2/J = 0.1$ data, the onset of long-range order shifts significantly when going from bond dimension 1000 to 2000 to 4000. While this is consistent in principle with an intermediate disordered phase, the apparent phase boundary would likely shift less if there were an underlying phase boundary than if it were simply an artifact of the fact that higher bond dimension decreases the energetic benefit of reducing entanglement by breaking symmetry and hence allows symmetry to be preserved even when further from the phase transition, where the energy cost of breaking symmetry is lower.

(2) We observe similar behavior for the two cuts, $J_2/J = 0$ and $J_2/J = 0.1$. As reviewed in Sec. II above, that there is a direct transition at $J_2 = 0$ is well established via a variety of numerical methods, most significantly iPEPS calculations that work directly in the thermodynamic limit [52]. The symmetry is preserved starting at a lower bond dimension for $J_2/J = 0.1$, which does leave open the possibility of a disordered phase, but it could just as well be the case that J_2 simply increases the energy cost of breaking the symmetry.

(3) If a disordered phase were indeed a spin liquid or Stiefel liquid, there would be some positive signatures beyond the mere absence of order. We have checked for topological order by performing flux insertion, which turns out to be 2π-periodic, thus ruling out spin fractionalization. We also added a scalar chirality term, $J_\chi \sum \mathbf{S} \cdot (\mathbf{S} \times \mathbf{S})$, to the Hamiltonian, which would cause a Dirac spin liquid and some Stiefel liquids to transition to a chiral spin liquid (CSL), possibly an $SU(3)_1$ CSL [98]. Instead, we observe no phase transition with small J_χ, and then a first-order transition to tetrahedral order with larger J_χ; see the Supplementary Material for more [96]. In short, signatures of likely spin liquid phases are not present.

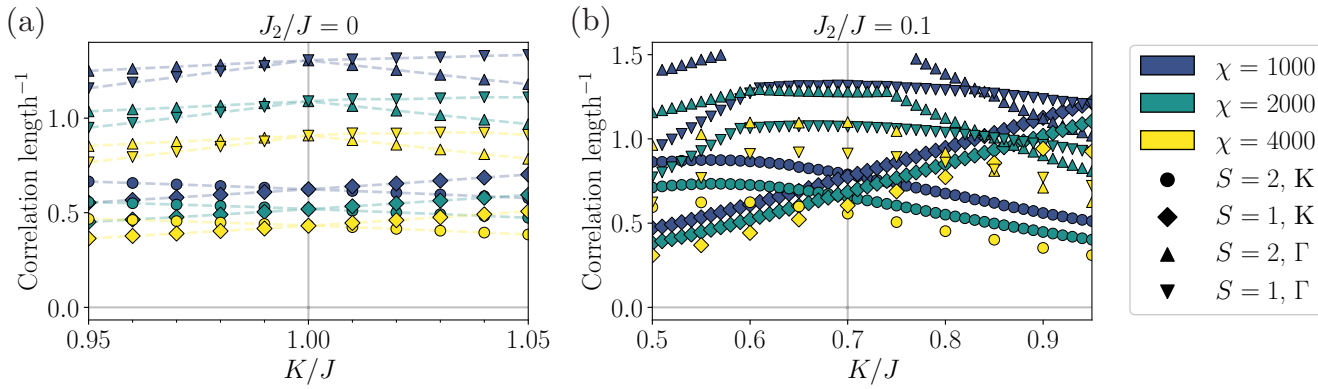

FIG. 8. Inverse correlation length for operators carrying total spin 1 and 2, with momentum corresponding to the Γ point ($\mathbf{k} = \mathbf{0}$) or the K points, for (a) $J_2 = 0$, and (b) $J_2/J = 0.1$. With $J_2 = 0$, for each (S, $\mathbf{k}$), the spin-1 and spin-2 correlation lengths are exactly equal when $K = J$ due to the emergent SU(3) symmetry. With $J_2/J = 0.1$, this is no longer true, and we identify the AFM-AFQ phase transition as the point where the largest spin-1 and largest spin-2 correlation lengths cross.

In summary, we cannot rigorously rule out the possibility of an intermediate disordered phase, which could be a spin liquid or a Stiefel liquid. However, in the absence of truly compelling evidence, we conclude that there is most likely a direct transition between the AFM and AFQ phases.

As part of this argument, we also suggested that the transition is not strongly first order, since if it were we could expect SSB to persist to higher bond dimensions near the transition, especially at $J_2/J = 0.1$. In fact, we can state unequivocally that there is no first-order transition between AFM and AFQ on the YC6 cylinder; we observe numerically that the MPS ground state evolves continuously from one phase to the other, with the overlap between the ground states at adjacent parameter points close to 1. This behavior on the cylinder does not rule out a weakly first-order transition in the two-dimensional model.

The continuous transition on the cylinder can be understood in part through correlation lengths for operators with different momentum and spin. In Fig. 8, we show the correlation lengths, for operators carrying $S = 1$ and $S = 2$ and corresponding to fluctuations with wave vectors at the K and Γ points, across the phase transition both at $J_2/J = 0$ and at $J_2/J = 0.1$; we briefly explain how to compute spin- and momentum-resolved correlation lengths in the Supplementary Material [96] using methods from Refs. [99–101]. The SU(3) symmetry when $J_2 = 0$, $K = J$ manifests in the exact equality of spin-1 and spin-2 correlation lengths, and this point is the phase transition between the magnetic and nematic orders. When $J_2/J = 0.1$, we likewise identify the parameter point where the longest correlation lengths for spin-1 and spin-2 cross as the phase transition, at $K \approx 0.7J$.

IV. DISCUSSION

We have numerically studied a highly frustrated model of interacting spin-1 degrees of freedom on the triangular lattice, with antiferromagnetic nearest- and next-nearest-neighbor interactions, and with nearest-neighbor biquadratic interactions. The biquadratic interactions can be reframed in terms of spin-quadrupole interactions, so that the Hamiltonian leads to competing spin-dipole and spin-quadrupole orders.

We find five ordered phases: 120° antiferromagnetic, stripe, and tetrahedral magnetic orders, and ferroquadrupolar and antiferroquadrupolar nematic orders. While the high degree of frustration in the model, due to competition both between nearest- and next-nearest-neighbor interaction and between magnetic and nematic order, could plausibly lead to spin liquid or Stiefel liquid ground states, our numerical results suggest that no such disordered state is in fact realized.

A natural follow-up question is how the model could be further modified to produce a spin liquid phase. The addition of single-ion anisotropy has been suggested as a possible route to spin-liquid behavior, especially with the additional inclusion of ring exchange [88] or anisotropy in the spin interactions [90,91]. Another interesting possibility is to explicitly target a nematic spin liquid by studying a model of purely quadrupole interactions, $\mathbf{Q}_v \cdot \mathbf{Q}_v$, including contributions beyond nearest-neighbor.

We also suggest that it would be useful to study the model including the next-nearest-neighbor interactions using inherently two-dimensional tensor network simulations, such as with iPEPS. In particular, since a continuous symmetry can be spontaneously broken in two dimensions even in the true ground state, such simulations would provide further confirmation that there is indeed no disordered state arising between the AFM and AFQ orders.

Finally, our result suggests that the AFM-AFQ transition may be continuous. If this is indeed true on a two-dimensional lattice, then the transition is guaranteed to be exotic (non-Landau) for two reasons: (1) The symmetry breaking patterns of the two phases are very different. In particular, the unbroken symmetry of either phase is not the subgroup of the other, so a Landau theory will not describe a direct continuous transition. (2) At the SU(3) symmetric point ($J_2 = 0$), the system has a Lieb-Schultz-Mattis (LSM) constraint because of the projective representation of PSU(3) per unit cell. The LSM constraint in turn requires any putative field theory of the phase transition to possess certain nontrivial 't Hooft anomaly, a feature clearly absent in any Landau theory.

Formulating such a putative theory of continuous AFM-AFQ transition is an interesting problem for future study.

ACKNOWLEDGMENTS

We thank Tim Hsieh and Weicheng Ye for helpful conversations. DMRG simulations were performed using the TenPy tensor network library [70], which includes significant contributions from Michael Zaletel, Roger Mong, and Frank Pollmann; an updated version of the library is publicly available [102]. Numerical computations were carried out using the Symmetry cluster at Perimeter Institute and the Cedar cluster at Simon Fraser University, through Compute Canada/the Digital Research Alliance of Canada. Research at Perimeter Institute is supported in part by the Government of Canada through the Department of Innovation, Science and Economic Development and by the Province of Ontario through the Ministry of Colleges and Universities. The carbon cost of the simulations reported in this paper was approximately 1.3 metric tons of CO_2.

APPENDIX: SPONTANEOUS SYMMETRY BREAKING AND BOND DIMENSION

Here we briefly address the question of how to interpret the presence or absence of spontaneous symmetry breaking in the MPS ground state at a given bond dimension. Our goal is to understand the case of a continuous symmetry on an infinite cylinder, but we first illustrate the key idea using a discrete symmetry on a finite one-dimensional system.

Consider, for concreteness, the transverse-field Ising model in one dimension:

$$H = \sum_i J\sigma_i^z\sigma_{i+1}^z + h\sigma_i^x, \tag{A1}$$

which has a $\mathbf{Z}_2$ symmetry: $(\bigotimes \sigma^x)H(\bigotimes \sigma^x) = H$. On a finite chain of length N, in the limit $J \gg h$, the two lowest-lying states are nearly degenerate, with splitting proportional to $(h/J)^N$. Both are eigenstates of the symmetry; in other words, in both the ground state and first excited state, symmetry is not spontaneously broken.

However, with a finite-bond-dimension MPS, it is possible for the lowest energy variational state to spontaneously break the symmetry. The bond dimension is the number of Schmidt values allowed to be nonzero on each bipartition of the state, and as the bond dimension increases, the variational space becomes larger and thus the lowest accessible energy becomes lower. A symmetry-preserving state will have Schmidt values in pairs, and the energy will be determined by the number of pairs kept. On the other hand, a corresponding symmetry-broken state will achieve the same energy with only half as many Schmidt values, or in other words will have lower energy when the Schmidt rank is the same. Consequently, at finite bond dimension there is an energy cost to preserving the symmetry, which we will call the "symmetry-entanglement gap."

Symmetry will be spontaneously broken if this gap is larger than the exponential splitting $(h/J)^N$. Infinite DMRG will thus spontaneously break discrete symmetry in one dimension (1D) for any bond dimension, since the true splitting is exactly zero and the symmetry-entanglement gap is merely tiny. Finite DMRG will break the symmetry up to some cutoff bond dimension, beyond which it will be restored.

We now turn to the more complicated case of a 2D model with a continuous symmetry, which is then restricted to a finite-circumference cylinder. The Mermin-Wagner theorem says that on this quasi-1D system, the true ground state cannot spontaneously break the symmetry. However, in DMRG simulations such SSB is possible, as we can understand by analogy with the 1D Ising model. The cylinder circumference plays the role of the 1D chain's length: when it becomes infinite, exact ground state degeneracy allows SSB to occur even in a true ground state, but when it is finite, the true ground state must be symmetry-preserving due to an energy splitting exponentially small in cylinder circumference. This splitting can be compared with the symmetry-entanglement gap due to finite bond dimension, with the result that even on a finite-circumference cylinder where the true ground state must respect the symmetry, the lowest-energy MPS will break the symmetry for sufficiently small bond dimension. Furthermore, the requisite bond dimension to preserve the symmetry will increase with cylinder circumference.

Suppose, on the other hand, that in the true two-dimensional ground state the continuous symmetry cannot be spontaneously broken, such as for a topological spin liquid. This implies an energy gap, Δ, above the symmetric ground state. If we view the main effect of finite cylinder circumference as restricting to certain momentum cuts in the Brillouin zone (which is a reasonable perspective when the circumference is large, less so when small), the corresponding gap on the cylinder will be comparable or larger. Hence for the lowest-energy MPS to spontaneously break the symmetry, we require the symmetry-entanglement gap to be larger than Δ. For any reasonable circumference, Δ will be substantially larger than the finite-circumference gap of a state with SSB, so that a continuous symmetry will only be broken when the bond dimension is quite small.

To summarize, with sufficiently small bond dimension the lowest-energy MPS on a finite-circumference, infinite-length cylinder will be expected to spontaneously break symmetry, regardless of what happens in the 2D model or the true ground state. However, if there is long-ranged order in 2D, the threshold bond dimension required to restore the symmetry on the cylinder will be larger than if the 2D ground state is disordered. Thus as a practical conclusion, we can guess that if a very large bond dimension is required in order to restore the symmetry, long-range order is likely present in 2D. Conversely, if the simulation setup allows the symmetry to be spontaneously broken but the symmetry is nonetheless respected even with very small bond dimension, then the 2D ground state likely has no long-ranged order.

[1] L. Balents, Spin liquids in frustrated magnets, Nature **464**, 199 (2010).

[2] L. Savary and L. Balents, Quantum spin liquids: A review, Rep. Prog. Phys. **80**, 016502 (2017).

[3] Y. Zhou, K. Kanoda, and T.-K. Ng, Quantum spin liquid states, Rev. Mod. Phys. **89**, 025003 (2017).

[4] P. Anderson, Resonating valence bonds: A new kind of insulator?, Mater. Res. Bull. **8**, 153 (1973).

[5] D. A. Huse and V. Elser, Simple Variational Wave Functions for Two-Dimensional Heisenberg Spin-1/2 Antiferromagnets, Phys. Rev. Lett. **60**, 2531 (1988).

[6] S. R. White and A. L. Chernyshev, Neél Order in Square and Triangular Lattice Heisenberg Models, Phys. Rev. Lett. **99**, 127004 (2007).

[7] Y. Shimizu, K. Miyagawa, K. Kanoda, M. Maesato, and G. Saito, Spin Liquid State in an Organic Mott Insulator with a Triangular Lattice, Phys. Rev. Lett. **91**, 107001 (2003).

[8] S. Yamashita, Y. Nakazawa, M. Oguni, Y. Oshima, H. Nojiri, Y. Shimizu, K. Miyagawa, and K. Kanoda, Thermodynamic properties of a spin-1/2 spin-liquid state in a κ-type organic salt, Nat. Phys. **4**, 459 (2008).

[9] M. Yamashita, N. Nakata, Y. Kasahara, T. Sasaki, N. Yoneyama, N. Kobayashi, S. Fujimoto, T. Shibauchi, and Y. Matsuda, Thermal-transport measurements in a quantum spin-liquid state of the frustrated triangular magnet κ-(BEDT-TTF)$_2$ $Cu_2(CN)_3$, Nat. Phys. **5**, 44 (2009).

[10] T. Itou, A. Oyamada, S. Maegawa, M. Tamura, and R. Kato, Quantum spin liquid in the spin-1/2 triangular antiferromagnet $EtMe_3$ $Sb[Pd(dmit)_2]_2$, Phys. Rev. B **77**, 104413 (2008).

[11] T. Itou, A. Oyamada, S. Maegawa, M. Tamura, and R. Kato, ^{13}C NMR study of the spin-liquid state in the triangular quantum antiferromagnet $EtMe_3$ $Sb[Pd(dmit)_2]_2$, J. Phys.: Conf. Ser. **145**, 012039 (2009).

[12] M. Yamashita, N. Nakata, Y. Senshu, M. Nagata, H. M. Yamamoto, R. Kato, T. Shibauchi, and Y. Matsuda, Highly mobile gapless excitations in a two-dimensional candidate quantum spin liquid, Science **328**, 1246 (2010).

[13] T. Itou, A. Oyamada, S. Maegawa, and R. Kato, Instability of a quantum spin liquid in an organic triangular-lattice antiferromagnet, Nat. Phys. **6**, 673 (2010).

[14] J. M. Ni, B. L. Pan, B. Q. Song, Y. Y. Huang, J. Y. Zeng, Y. J. Yu, E. J. Cheng, L. S. Wang, D. Z. Dai, R. Kato, and S. Y. Li, Absence of Magnetic Thermal Conductivity in the Quantum Spin Liquid Candidate $EtMe_3$ $Sb[Pd(dmit)_2]_2$, Phys. Rev. Lett. **123**, 247204 (2019).

[15] P. Bourgeois-Hope, F. Laliberté, E. Lefrançois, G. Grissonnanche, S. R. de Cotret, R. Gordon, S. Kitou, H. Sawa, H. Cui, R. Kato, L. Taillefer, and N. Doiron-Leyraud, Thermal Conductivity of the Quantum Spin Liquid Candidate $EtMe_3$ $Sb[Pd(dmit)_2]_2$: No Evidence of Mobile Gapless Excitations, Phys. Rev. X **9**, 041051 (2019).

[16] M. Yamashita, Boundary-limited and glassy-like phonon thermal conduction in $EtMe_3$ $Sb[Pd(dmit)_2]_2$, J. Phys. Soc. Jpn. **88**, 083702 (2019).

[17] Y.-D. Li, Y. Shen, Y. Li, J. Zhao, and G. Chen, Effect of spin-orbit coupling on the effective-spin correlation in $YbMgGaO_4$, Phys. Rev. B **97**, 125105 (2018).

[18] Y. Shen, Y.-D. Li, H. Wo, Y. Li, S. Shen, B. Pan, Q. Wang, H. C. Walker, P. Steffens, M. Boehm, Y. Hao, D. L. Quintero-Castro, L. W. Harriger, M. D. Frontzek, L. Hao, S. Meng, Q. Zhang, G. Chen, and J. Zhao, Evidence for a spinon Fermi surface in a triangular-lattice quantum-spin-liquid candidate, Nature **540**, 559 (2016).

[19] Y. Shen, Y.-D. Li, H. C. Walker, P. Steffens, M. Boehm, X. Zhang, S. Shen, H. Wo, G. Chen, and J. Zhao, Fractionalized excitations in the partially magnetized spin liquid candidate $YbMgGaO_4$, Nat. Commun. **9**, 4138 (2018).

[20] J. S. Helton, K. Matan, M. P. Shores, E. A. Nytko, B. M. Bartlett, Y. Yoshida, Y. Takano, A. Suslov, Y. Qiu, J.-H. Chung, D. G. Nocera, and Y. S. Lee, Spin Dynamics of the Spin-1/2 Kagome Lattice Antiferromagnet $ZnCu_3(OH)_6$ Cl_2, Phys. Rev. Lett. **98**, 107204 (2007).

[21] T.-H. Han, J. S. Helton, S. Chu, D. G. Nocera, J. A. Rodriguez-Rivera, C. Broholm, and Y. S. Lee, Fractionalized excitations in the spin-liquid state of a kagome-lattice antiferromagnet, Nature **492**, 406 (2012).

[22] Y. Iqbal, W.-J. Hu, R. Thomale, D. Poilblanc, and F. Becca, Spin liquid nature in the Heisenberg $J_1 - J_2$ triangular antiferromagnet, Phys. Rev. B **93**, 144411 (2016).

[23] S. Hu, W. Zhu, S. Eggert, and Y.-C. He, Dirac Spin Liquid on the Spin-1/2 Triangular Heisenberg Antiferromagnet, Phys. Rev. Lett. **123**, 207203 (2019).

[24] A. Szasz, J. Motruk, M. P. Zaletel, and J. E. Moore, Chiral Spin Liquid Phase of the Triangular Lattice Hubbard Model: A Density Matrix Renormalization Group Study, Phys. Rev. X **10**, 021042 (2020).

[25] A. Szasz and J. Motruk, Phase diagram of the anisotropic triangular lattice hubbard model, Phys. Rev. B **103**, 235132 (2021).

[26] T. Cookmeyer, J. Motruk, and J. E. Moore, Four-Spin Terms and the Origin of the Chiral Spin Liquid in Mott Insulators on the Triangular Lattice, Phys. Rev. Lett. **127**, 087201 (2021).

[27] B.-B. Chen, Z. Chen, S.-S. Gong, D. N. Sheng, W. Li, and A. Weichselbaum, Quantum spin liquid with emergent chiral order in the triangular-lattice hubbard model, arXiv:2102.05560 (2021).

[28] Y. Zhou, D. N. Sheng, and E.-A. Kim, Quantum Phases of Transition Metal Dichalcogenide Moiré Systems, Phys. Rev. Lett. **128**, 157602 (2022).

[29] Y. Ran, M. Hermele, P. A. Lee, and X.-G. Wen, Projected-Wave-Function Study of the Spin-1/2 Heisenberg Model on the Kagomé Lattice, Phys. Rev. Lett. **98**, 117205 (2007).

[30] Y. Iqbal, F. Becca, S. Sorella, and D. Poilblanc, Gapless spin-liquid phase in the kagome spin-$\frac{1}{2}$ Heisenberg antiferromagnet, Phys. Rev. B **87**, 060405(R) (2013).

[31] Y.-C. He, D. N. Sheng, and Y. Chen, Chiral Spin Liquid in a Frustrated Anisotropic Kagome Heisenberg Model, Phys. Rev. Lett. **112**, 137202 (2014).

[32] S.-S. Gong, W. Zhu, and D. N. Sheng, Emergent chiral spin liquid: Fractional quantum Hall effect in a Kagome Heisenberg model, Sci. Rep. **4**, 6317 (2014).

[33] Y.-C. He, M. P. Zaletel, M. Oshikawa, and F. Pollmann, Signatures of Dirac Cones in a DMRG Study of the Kagome Heisenberg Model, Phys. Rev. X **7**, 031020 (2017).

[34] S. Nakatsuji, Y. Nambu, H. Tonomura, O. Sakai, S. Jonas, C. Broholm, H. Tsunetsugu, Y. Qiu, and Y. Maeno, Spin disorder on a triangular lattice, Science **309**, 1697 (2005).

[35] Y. Nambu, S. Nakatsuji, and Y. Maeno, Coherent behavior and nonmagnetic impurity effects of spin disordered state in $NiGa_2$ S_4, J. Phys. Soc. Jpn. **75**, 043711 (2006).

[36] S. Nakatsuji, Y. Nambu, K. Onuma, S. Jonas, C. Broholm, and Y. Maeno, Coherent behaviour without magnetic order of the triangular lattice antiferromagnet $NiGa_2S_4$, J. Phys.: Condens. Matter **19**, 145232 (2007).

[37] H. Takeya, K. Ishida, K. Kitagawa, Y. Ihara, K. Onuma, Y. Maeno, Y. Nambu, S. Nakatsuji, D. E. MacLaughlin, A. Koda, and R. Kadono, Spin dynamics and spin freezing behavior in the two-dimensional antiferromagnet $NiGa_2S_4$ revealed by Ga-NMR, NQR and μSR measurements, Phys. Rev. B **77**, 054429 (2008).

[38] D. E. MacLaughlin, Y. Nambu, S. Nakatsuji, R. H. Heffner, L. Shu, O. O. Bernal, and K. Ishida, Unconventional spin freezing and fluctuations in the frustrated antiferromagnet $NiGa_2S_4$, Phys. Rev. B **78**, 220403(R) (2008).

[39] S. Nakatsuji, Y. Nambu, and S. Onoda, Novel geometrical frustration effects in the two-dimensional triangular-lattice antiferromagnet $NiGa_2S_4$ and related compounds, J. Phys. Soc. Jpn. **79**, 011003 (2010).

[40] D. E. MacLaughlin, Y. Nambu, Y. Ohta, Y. Machida, S. Nakatsuji, and O. O. Bernal, Muons and frustrated magnetism in $NiGa_2S_4$ and $Pr_2Ir_2O_7$, J. Phys.: Conf. Ser. **225**, 012031 (2010).

[41] I. I. Mazin, Ab initio investigation of magnetic interactions in the frustrated triangular magnet $NiGa_2S_4$, Phys. Rev. B **76**, 140406(R) (2007).

[42] K. Takubo, T. Mizokawa, J.-Y. Son, Y. Nambu, S. Nakatsuji, and Y. Maeno, Unusual Superexchange Pathways in an NiS_2 Triangular Lattice with Negative Charge-Transfer Energy, Phys. Rev. Lett. **99**, 037203 (2007).

[43] K. Takubo, T. Mizokawa, Y. Nambu, and S. Nakatsuji, Electronic structure study of triangular lattices in $FeGa_2S_4$, $Fe_2Ga_2S_5$, and $NiGa_2S_4$: Photoemission spectroscopy and hartree-fock calculations, Phys. Rev. B **79**, 134422 (2009).

[44] H. Takenaka, K. Nagata, T. Mizokawa, and M. Okada, Model selection of $NiGa_2S_4$ triangular lattice by bayesian inference, J. Phys. Soc. Jpn. **83**, 124706 (2014).

[45] H. Takenaka, K. Nagata, T. Mizokawa, and M. Okada, Bayesian approach to effective model of $NiGa_2S_4$ triangular lattice with boltzmann factor, J. Phys. Soc. Jpn. **85**, 124003 (2016).

[46] A. V. Chubukov, Fluctuations in spin nematics, J. Phys.: Condens. Matter **2**, 1593 (1990).

[47] A. Kartsev, M. Augustin, R. F. L. Evans, K. S. Novoselov, and E. J. G. Santos, Biquadratic exchange interactions in two-dimensional magnets, npj Comput. Mater. **6**, 150 (2020).

[48] H. Tsunetsugu and M. Arikawa, Spin nematic phase in $S = 1$ triangular antiferromagnets, J. Phys. Soc. Jpn. **75**, 083701 (2006).

[49] A. Läuchli, F. Mila, and K. Penc, Quadrupolar Phases of the $S = 1$ Bilinear-Biquadratic Heisenberg Model on the Triangular Lattice, Phys. Rev. Lett. **97**, 087205 (2006).

[50] M. Moreno-Cardoner, H. Perrin, S. Paganelli, G. De Chiara, and A. Sanpera, Case study of the uniaxial anisotropic spin-1 bilinear-biquadratic Heisenberg model on a triangular lattice, Phys. Rev. B **90**, 144409 (2014).

[51] I. Niesen and P. Corboz, A tensor network study of the complete ground state phase diagram of the spin-1 bilinear-biquadratic Heisenberg model on the square lattice, SciPost Phys. **3**, 030 (2017).

[52] I. Niesen and P. Corboz, Ground-state study of the spin-1 bilinear-biquadratic Heisenberg model on the triangular lattice using tensor networks, Phys. Rev. B **97**, 245146 (2018).

[53] S. Bhattacharjee, V. B. Shenoy, and T. Senthil, Possible ferro-spin nematic order in $NiGa_2S_4$, Phys. Rev. B **74**, 092406 (2006).

[54] H. Tsunetsugu and M. Arikawa, The spin nematic state in triangular antiferromagnets, J. Phys.: Condens. Matter **19**, 145248 (2007).

[55] Y. Doi, Y. Hinatsu, and K. Ohoyama, Structural and magnetic properties of pseudo-two-dimensional triangular antiferromagnets $Ba_3MSb_2O_9$(M=Mn, Co, and Ni), J. Phys.: Condens. Matter **16**, 8923 (2004).

[56] J. G. Cheng, G. Li, L. Balicas, J. S. Zhou, J. B. Goodenough, C. Xu, and H. D. Zhou, High-Pressure Sequence of $Ba_3NiSb_2O_9$ Structural Phases: New $S = 1$ Quantum Spin Liquids Based on Ni^{2+}, Phys. Rev. Lett. **107**, 197204 (2011).

[57] T. Ono, H. Tanaka, Y. Shirata, A. Matsuo, K. Kindo, F. Ishikawa, O. Kolomiyets, H. Mitamura, T. Goto, H. Nakano, N. A. Fortune, S. T. Hannahs, Y. Yoshida, and Y. Takano, Magnetic-field induced quantum phase transitions in triangular-lattice antiferromagnets, J. Phys.: Conf. Ser. **302**, 012003 (2011).

[58] Y. Shirata, H. Tanaka, T. Ono, A. Matsuo, K. Kindo, and H. Nakano, Quantum magnetization plateau in spin-1 triangular-lattice antiferromagnet $Ba_3NiSb_2O_9$, J. Phys. Soc. Jpn. **80**, 093702 (2011).

[59] J. A. Quilliam, F. Bert, A. Manseau, C. Darie, C. Guillot-Deudon, C. Payen, C. Baines, A. Amato, and P. Mendels, Gapless quantum spin liquid ground state in the spin-1 antiferromagnet $6HB - Ba_3NiSb_2O_9$, Phys. Rev. B **93**, 214432 (2016).

[60] B. Fåk, S. Bieri, E. Canévet, L. Messio, C. Payen, M. Viaud, C. Guillot-Deudon, C. Darie, J. Ollivier, and P. Mendels, Evidence for a spinon fermi surface in the triangular $S = 1$ quantum spin liquid $Ba_3NiSb_2O_9$, Phys. Rev. B **95**, 060402(R) (2017).

[61] M. Saito, M. Watanabe, N. Kurita, A. Matsuo, K. Kindo, M. Avdeev, H. O. Jeschke, and H. Tanaka, Successive phase transitions and magnetization plateau in the spin-1 triangular-lattice antiferromagnet $Ba_2La_2NiTe_2O_{12}$ with small easy-axis anisotropy, Phys. Rev. B **100**, 064417 (2019).

[62] N. Li, Q. Huang, A. Brassington, X. Y. Yue, W. J. Chu, S. K. Guang, X. H. Zhou, P. Gao, E. X. Feng, H. B. Cao, E. S. Choi, Y. Sun, Q. J. Li, X. Zhao, H. D. Zhou, and X. F. Sun, Quantum spin state transitions in the spin-1 equilateral triangular lattice antiferromagnet $Na_2BaNi(PO_4)_2$, Phys. Rev. B **104**, 104403 (2021).

[63] X. Bai, S.-S. Zhang, Z. Dun, H. Zhang, Q. Huang, H. Zhou, M. B. Stone, A. I. Kolesnikov, F. Ye, C. D. Batista, and M. Mourigal, Hybridized quadrupolar excitations in the spin-anisotropic frustrated magnet FeI_2, Nat. Phys. **17**, 467 (2021).

[64] Y. Yu and S. A. Kivelson, Phases of frustrated quantum antiferromagnets on the square and triangular lattices, Phys. Rev. B **101**, 214404 (2020).

[65] L. Zou, Y.-C. He, and C. Wang, Stiefel Liquids: Possible Non-Lagrangian Quantum Criticality from Intertwined Orders, Phys. Rev. X **11**, 031043 (2021).

[66] W. Ye, M. Guo, Y.-C. He, C. Wang, and L. Zou, Topological characterization of lieb-schultz-mattis constraints

and applications to symmetry-enriched quantum criticality, arXiv:2111.12097 (2021).

[67] S. R. White, Density Matrix Formulation for Quantum Renormalization Groups, Phys. Rev. Lett. **69**, 2863 (1992).

[68] S. R. White, Density-matrix algorithms for quantum renormalization groups, Phys. Rev. B **48**, 10345 (1993).

[69] U. Schollwöck, The density-matrix renormalization group in the age of matrix product states, Ann. Phys. **326**, 96 (2011).

[70] J. A. Kjäll, M. P. Zaletel, R. S. K. Mong, J. H. Bardarson, and F. Pollmann, Phase diagram of the anisotropic spin-2 XXZ model: Infinite-system density matrix renormalization group study, Phys. Rev. B **87**, 235106 (2013).

[71] C. Hubig, I. P. McCulloch, and U. Schollwöck, Generic construction of efficient matrix product operators, Phys. Rev. B **95**, 035129 (2017).

[72] M. Blume and Y. Y. Hsieh, Biquadratic exchange and quadrupolar ordering, J. Appl. Phys. **40**, 1249 (1969).

[73] H. H. Chen and P. M. Levy, Quadrupole Phase Transitions in Magnetic Solids, Phys. Rev. Lett. **27**, 1383 (1971).

[74] V. Matveev, Quantum quadrupolar magnetism and phase transitions in the presence of biquadratic exchange, Zh. Eksp. Teor. Fiz. **65**, 1626 (1974) [JETP **38**, 813 (1974)].

[75] A. Andreev and I. Grishchuk, Spin nematics, Zh. Eksp. Teor. Fiz. **87**, 467 (1984) [Sov. Phys. JETP **60**, 267 (1984)].

[76] N. Papanicolaou, Unusual phases in quantum spin-1 systems, Nucl. Phys. B **305**, 367 (1988).

[77] The factor of $\sqrt{2}$ on the left-hand side is included for consistency with $\mathbf{Q}_v$, Eq. (4). Note that some past works, such as Ref. [79], define $\mathbf{Q}$ without this $\sqrt{2}$.

[78] For a single-site state $d_x|x\rangle + d_y|y\rangle + d_z|z\rangle$, we have $\langle S_\alpha S_\beta\rangle = \delta_{\alpha\beta} - d^*_\alpha d_\beta$ [91], and thus $\langle \mathbf{Q}_v\rangle^2 = 4/3 - 4(\mathrm{Im}[d^*_x d_y]^2 + \mathrm{Im}[d^*_y d_z]^2 + \mathrm{Im}[d^*_z d_x]^2)$, which is manifestly upper-bounded by $4/3$.

[79] R. K. Kaul, Spin nematic ground state of the triangular lattice $S = 1$ biquadratic model, Phys. Rev. B **86**, 104411 (2012).

[80] Note that the center of SU(3), which is $\mathbf{Z}_3$ generated by $e^{i2\pi/3}\mathrm{Id}$, acts trivially on the local degrees of freedom, so technically the symmetry group is SU(3)/$\mathbf{Z}_3$. However, this subtlety is not important for our results.

[81] M. Gell-Mann, Symmetries of baryons and mesons, Phys. Rev. **125**, 1067 (1962).

[82] P. Li, G.-M. Zhang, and S.-Q. Shen, Su(3) bosons and the spin nematic state on the spin-1 bilinear-biquadratic triangular lattice, Phys. Rev. B **75**, 104420 (2007).

[83] A. Smerald and N. Shannon, Theory of spin excitations in a quantum spin-nematic state, Phys. Rev. B **88**, 184430 (2013).

[84] B. Bauer, P. Corboz, A. M. Läuchli, L. Messio, K. Penc, M. Troyer, and F. Mila, Three-sublattice order in the SU(3) Heisenberg model on the square and triangular lattice, Phys. Rev. B **85**, 125116 (2012).

[85] X.-T. Zhang, W.-J. Hu, E. Dagotto, and S. Gong, Fragility of the nematic spin liquid induced by diagonal couplings in the square-lattice SU(3) model, Phys. Rev. B **104**, 195135 (2021).

[86] W.-J. Hu, S.-S. Gong, H.-H. Lai, H. Hu, Q. Si, and A. H. Nevidomskyy, Nematic spin liquid phase in a frustrated spin-1 system on the square lattice, Phys. Rev. B **100**, 165142 (2019).

[87] W.-J. Hu, S.-S. Gong, H.-H. Lai, Q. Si, and E. Dagotto, Density matrix renormalization group study of nematicity in two dimensions: Application to a spin-1 bilinear-biquadratic model on the square lattice, Phys. Rev. B **101**, 014421 (2020).

[88] S. Bieri, M. Serbyn, T. Senthil, and P. A. Lee, Paired chiral spin liquid with a fermi surface in $S = 1$ model on the triangular lattice, Phys. Rev. B **86**, 224409 (2012).

[89] M. Serbyn, T. Senthil, and P. A. Lee, Exotic $S = 1$ spin-liquid state with fermionic excitations on the triangular lattice, Phys. Rev. B **84**, 180403(R) (2011).

[90] Z. Wang, A. E. Feiguin, W. Zhu, O. A. Starykh, A. V. Chubukov, and C. D. Batista, Chiral liquid phase of simple quantum magnets, Phys. Rev. B **96**, 184409 (2017).

[91] U. F. P. Seifert and L. Savary, Phase diagrams and excitations of anisotropic $S = 1$ quantum magnets on the triangular lattice, arXiv:2203.13490 (2022).

[92] T. Grover and T. Senthil, Non-Abelian Spin Liquid in a Spin-One Quantum Magnet, Phys. Rev. Lett. **107**, 077203 (2011).

[93] E. M. Stoudenmire, S. Trebst, and L. Balents, Quadrupolar correlations and spin freezing in $S = 1$ triangular lattice antiferromagnets, Phys. Rev. B **79**, 214436 (2009).

[94] Z.-X. Liu, Y. Zhou, and T.-K. Ng, Possibility of $S = 1$ spin liquids with fermionic spinons on triangular lattices, Phys. Rev. B **81**, 224417 (2010).

[95] P. Rubin, A. Sherman, and M. Schreiber, The spin-1 two-dimensional $J_1 - J_2$ Heisenberg antiferromagnet on a triangular lattice, Phys. Lett. A **374**, 3567 (2010).

[96] See Supplemental Material at http://link.aps.org/supplemental/10.1103/PhysRevB.106.115103 for the main text.

[97] L. Cincio and G. Vidal, Characterizing Topological Order by Studying the Ground States on an Infinite Cylinder, Phys. Rev. Lett. **110**, 067208 (2013).

[98] J.-Y. Chen, J.-W. Li, P. Nataf, S. Capponi, M. Mambrini, K. Totsuka, H.-H. Tu, A. Weichselbaum, J. von Delft, and D. Poilblanc, Abelian SU(N)$_1$ chiral spin liquids on the square lattice, Phys. Rev. B **104**, 235104 (2021).

[99] F. Pollmann and A. M. Turner, Detection of symmetry-protected topological phases in one dimension, Phys. Rev. B **86**, 125441 (2012).

[100] V. Zauner, D. Draxler, L. Vanderstraeten, M. Degroote, J. Haegeman, M. M. Rams, V. Stojevic, N. Schuch, and F. Verstraete, Transfer matrices and excitations with matrix product states, New J. Phys. **17**, 053002 (2015).

[101] M. Gohlke, G. Wachtel, Y. Yamaji, F. Pollmann, and Y. B. Kim, Quantum spin liquid signatures in Kitaev-like frustrated magnets, Phys. Rev. B **97**, 075126 (2018).

[102] J. Hauschild and F. Pollmann, Efficient numerical simulations with tensor networks: Tensor Network Python (TeNPy), SciPost Phys. Lect. Notes, 5 (2018).